

Insights into the Nitric Oxide Reductase Mechanism of Flavodiiron Proteins from a Flavin-Free Enzyme[†]

Takahiro Hayashi,^{‡,||} Jonathan D. Caranto,^{§,||} David A. Wampler,[§] Donald M. Kurtz, Jr.,^{*,§} and Pierre Moënne-Loccoz^{*,‡}

[‡]Department of Science and Engineering, School of Medicine, Oregon Health and Science University, 20000 Northwest Walker Road, Beaverton, Oregon 97006, and [§]Department of Chemistry, University of Texas, San Antonio, Texas 78249. ^{||}These authors contributed equally to this work.

Received May 18, 2010; Revised Manuscript Received July 14, 2010

ABSTRACT: Flavodiiron proteins (FDPs) catalyze reductive scavenging of dioxygen and nitric oxide in air-sensitive microorganisms. FDPs contain a distinctive non-heme diiron/flavin mononucleotide (FMN) active site. Alternative mechanisms for the nitric oxide reductase (NOR) activity consisting of either protonation of a diiron-bridging hyponitrite or “super-reduction” of a diferrous-dinitrosyl by the proximal FMNH₂ in the rate-determining step have been proposed. To test these alternative mechanisms, we examined a deflavinated FDP (deflavo-FDP) from *Thermotoga maritima*. The deflavo-FDP retains an intact diiron site but does not exhibit multiturnover NOR or O₂ reductase (O₂R) activity. Reactions of the reduced (diferrous) deflavo-FDP with nitric oxide were examined by UV–vis absorption, EPR, resonance Raman, and FTIR spectroscopies. Anaerobic addition of nitric oxide up to one NO per diferrous deflavo-FDP results in formation of a diiron–mononitrosyl complex characterized by a broad $S = 1/2$ EPR signal arising from antiferromagnetic coupling of an $S = 3/2$ {FeNO}⁷ with an $S = 2$ Fe(II). Further addition of NO results in two reaction pathways, one of which produces N₂O and the diferric site and the other of which produces a stable diiron–dinitrosyl complex. Both NO-treated and as-isolated deflavo-FDPs regain full NOR and O₂R activities upon simple addition of FMN. The production of N₂O upon addition of NO to the mononitrosyl deflavo-FDP supports the hyponitrite mechanism, but the concomitant formation of a stable diiron–dinitrosyl complex in the deflavo-FDP is consistent with a super-reduction pathway in the flavinated enzyme. We conclude that a diiron–mononitrosyl complex is an intermediate in the NOR catalytic cycle of FDPs.

Flavodiiron proteins (FDPs)¹ are widespread among bacteria, archaea, and some protozoan pathogens (1–6). FDPs play important roles in the responses to oxidative and nitrosative stresses in microaerobic and anoxic environments by reductively scavenging dioxygen and nitric oxide according to Scheme 1.

The relative levels of NADH:dioxygen reductase (O₂R) versus NADH:nitric oxide oxidoreductase (NOR) activities (at saturating NROR/Rd) vary significantly among FDPs, but these variations have yet to be correlated with specific structural features. FDPs are soluble cytoplasmic enzymes that are unrelated to the membrane-bound denitrifying NORs (7–9). The minimum

functional unit of all structurally characterized FDPs is a “head-to-tail” homodimer (Figure 1) (6, 10, 11). The N-terminal domain of each subunit contains a non-heme diiron site (Fe1–Fe2 distance 3.2–3.6 Å), while the C-terminal domain binds a flavin mononucleotide (FMN) cofactor ~4 Å from the diiron site in the opposite subunit (Figure 1). In almost all structurally characterized FDPs, each iron of the diiron site contains two histidine ligands and a terminal monodentate carboxylate ligand from either aspartate or glutamate. Bridging aspartate carboxylate and oxo/hydroxo ligands complete the diiron coordination sphere, resulting in two five-coordinate irons. Solvent or other exogenous small molecules occupy a buried pocket above the diiron site in these FDP structures. An obvious inference is that O₂ or NO diffuses into this pocket and binds to the sixth iron coordination sites during enzymatic turnover. Minimal O₂R and NOR mechanisms can thus be envisioned involving precursor diferrous–substrate complexes leading to reductive formation of either water from O₂ or N₂O from NO. According to the reaction stoichiometry (Scheme 1), a single O₂R turnover requires four reducing equivalents (presumably provided endogenously by the diferrous site and proximal FMNH₂), whereas a single NOR turnover requires only two reducing equivalents.

The His/carboxylate/solvent-bridged diiron sites of FDPs are reminiscent of those in subunit R2 of ribonucleotide reductase (12–15), the hydroxylase component of soluble methane monooxygenase (MMOH) (16–18), and the Δ⁹-stearoyl-acyl carrier protein desaturase (Δ⁹D) (19, 20), although there is no

[†]This work was supported in part by the National Institutes of Health (Grant GM74785 to P.M.-L. and Grant GM040388 to D.M.K.) and a Vertex pharmaceutical scholarship for T.H.

*To whom correspondence should be addressed. P.M.-L.: Department of Science and Engineering, School of Medicine, Oregon Health and Science University, 20000 NW Walker Rd., Beaverton, OR 97006; telephone, (503) 748-1673; fax, (503) 748-1464; e-mail, plocco@ebs.ogi.edu. D.M.K.: Department of Chemistry, University of Texas, San Antonio, TX 78249; telephone, (210) 458-7060; fax, (210) 458-7428; e-mail, donald.kurtz@utsa.edu.

Abbreviations: FDP, flavodiiron protein; FMN, flavin mononucleotide; *Mt*, *Moorella thermoacetica*; *Tm*, *Thermotoga maritima*; MMOH, hydroxylase component of soluble methane monooxygenase; Δ⁹D, Δ⁹-stearoyl-acyl carrier protein desaturase; EPR, electron paramagnetic resonance; RR, resonance Raman; FTIR, Fourier transform infrared; Rd, rubredoxin; NROR, NADH:rubredoxin oxidoreductase; PDB, Protein Data Bank; XDK, *m*-xylylenediamine bis(Kemp’s triacid)imide; MOPS, 3-(*N*-morpholino)propanesulfonic acid; O/N, oxygen/nitrogen; Et-HPTB, *N,N,N',N'*-tetrakis(*N*-ethyl-2-benzimidazolylmethyl)-1,3-diaminopropane; TMPD, *N,N,N',N'*-tetramethyl-*p*-phenylenediamine.

detectable amino acid sequence homology between any of these latter enzymes and FDPs. While the diferrous sites of both MMOH and R2 form NO adducts, neither of these proteins exhibits significant NOR activity (21–23). The NO adduct of

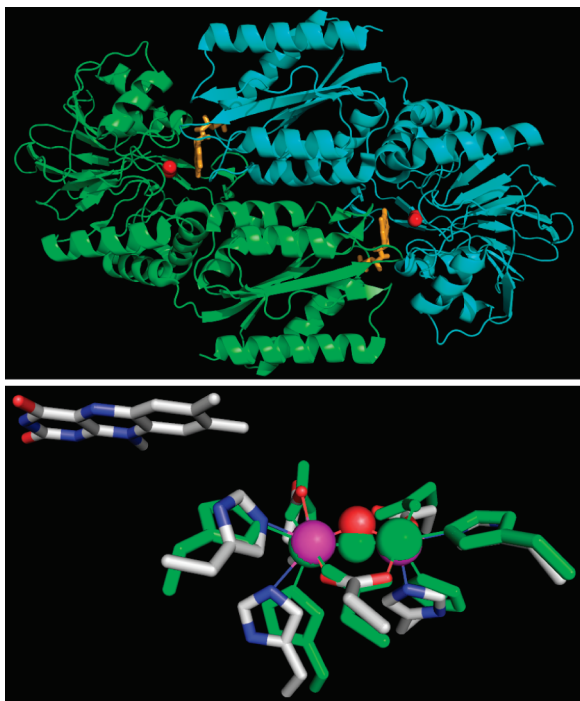
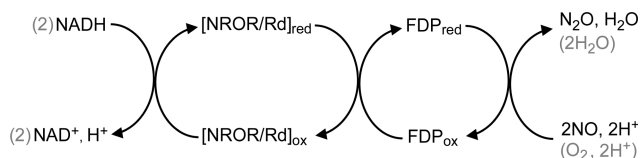
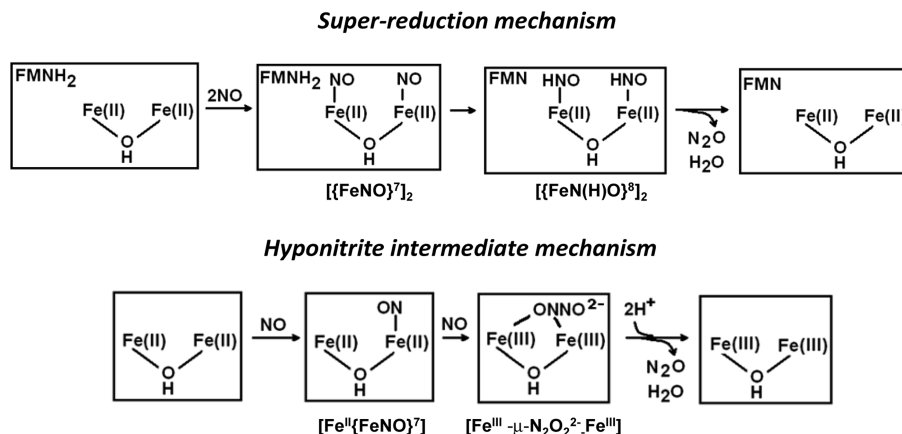


FIGURE 1: (Top) Homodimeric backbone structure of *Moorella thermoacetica* FDP (PDB entry 1YCF) showing iron atoms as red spheres and FMN as orange sticks. (Bottom) Superposition of the diiron sites in *Mt* FDP (PDB entry 1YCF) and *Tm* FDP (PDB entry 1VME). For the *Mt* FDP diiron site, iron ligand side chains are depicted as CPK-colored sticks, irons are depicted as purple spheres, and bridging solvent is depicted as a red sphere. All corresponding *Tm* FDP atoms are colored green. The proximal isoalloxazine ring of FMN in *Mt* FDP is also shown. Images and superposition were generated in PyMOL (DeLano Scientific LLC).

Scheme 1



Scheme 2



reduced R2 was characterized as a symmetric, magnetically coupled diferrous-dinitrosyl (21, 23) $[\{FeNO\}^7]_2$ in the notation of Enemark and Feltham (24)]. The reasons for the striking difference in reactivity toward NO of seemingly similar diiron sites in FDPs versus other non-heme diiron proteins are unclear. One possible explanation is that the proximal FMN cofactor in FDP plays a more integral role in the catalytic turnover than simply re-reducing the diiron site back to diferrous after its oxidation to the diferric state by two NO molecules. Super-reduction of a diferrous–dinitrosyl precursor to a ferrous–nitroxyl or a diferrous–dinitroxyl complex, i.e., $[\{FeN(H)O\}^8 \cdot \{FeNO\}^7]$ or $[\{FeN(H)O\}^8]_2$, respectively, by the proximal FMNH₂ has been proposed as an energetically favorable route for proton delivery and N–N bond formation leading to the release of N₂O and water (Scheme 2) (5, 11). A computational study, however, suggested an alternative mechanism in which the binding of NO to one iron forms a diiron–mononitrosyl complex before the $\{FeNO\}^7$ unit reacts with a second NO to produce a diferric–hyponitrite intermediate (Scheme 2) (25). An analogous hyponitrite pathway is also presumed to occur in the denitrifying NORs (8, 26–28).

Thus, in the super-reduction mechanism, FMNH₂ is essential for turnover of the diferrous–dinitrosyl intermediate, whereas in the hyponitrite intermediate mechanism, protonation of the spontaneously formed diferric–hyponitrite intermediate leads directly to release of N₂O without the participation of the FMN. In principle, these mechanisms could be distinguished by examining the reactivity of the diiron site with NO in the absence of the FMN cofactor. In 2004, a crystal structure of an FDP from the thermophilic bacterium *Thermotoga maritima* (*Tm*) was deposited in the Protein Data Bank (entry 1VME) by the Joint Center for Structural Genomics. The diiron site structure in *Tm* FDP is very similar to that in other FDPs (Figure 1), but the proximal FMN cofactor is absent in the deposited *Tm* FDP structure. This latter structure, thus, suggests the possibility of characterizing the reactivity of the diiron site in the flavin-free *Tm* FDP.

Tm is classified as an anaerobic bacterium. Elevated *Tm* FDP levels are observed in *Tm* cultures exposed to low levels of dioxygen, suggesting a role for this FDP in oxidative stress protection (29). We have found no reports of the response of *Tm* to nitric oxide exposure or of reactions of *Tm* FDP with nitric oxide. In this study, we show that flavin-containing *Tm* FDP has NOR activity and characterize the reactions of the FMN-free *Tm* FDP (deflavo-FDP) with nitric oxide.

MATERIALS AND METHODS

Protein Preparations. All protein concentrations are expressed either in monomers or, where indicated, on the basis of FMN content. The expression and purification of recombinant *Tm* FDP (GeneID TM0755), *Tm* rubredoxin (Rd), and *Tm* NADH:rubredoxin oxidoreductase (NROR) (31) and iron, protein, and flavin analyses (3, 30) were conducted as described elsewhere.

FDP Deflavination and Re flavination. Approximately 20 mg of as-isolated *Tm* FDP was applied to a 50 mL Phenyl Sepharose column (GE Healthcare) with buffer A [50 mM MOPS, 100 mM Na₂HPO₄, 100 mM KC₂H₃O₂, and 1.2 M NH₄SO₄ (pH 7.4)] to immobilize the FDP. The column pH was then lowered using a 20 column-volume gradient from buffer A to buffer B [50 mM MOPS, 100 mM Na₂HPO₄, 100 mM KC₂H₃O₂, and 1.2 M NH₄SO₄ (pH 2.5)]. FMN (yellow band) was eluted from the column at pH 2.5 with buffer B. The column pH was returned to pH 7.3 using a 20 column volume gradient from buffer B to buffer A. The deflavinated FDP (deflavo-FDP) was eluted with 50 mM MOPS (pH 7.3). The eluted deflavo-FDP was washed with 50 mM MOPS (pH 7.3) in an Amicon 30000 NMWL centrifugal filter unit (Millipore), and the protein was stored in 50 mM MOPS (pH 7.4). Deflavo-FDP was quantitatively re flavinated (reflavo-FDP) by incubation of a 5:1 FMN/deflavo-FDP (in monomer) mixture (approximate [FDP] = 2 mM) at 37 °C for ~15 min. Excess FMN was removed by centrifugal filtration washing with 50 mM MOPS (pH 7.3) until the flow-through was colorless. In situ re flavination was accomplished as described below.

O₂R/NOR Activity Assays and N₂O Production Measurements. NADH-dependent O₂R and NOR activities were measured spectrophotometrically by monitoring NADH consumption rates ($\epsilon_{340} = 6220 \text{ M}^{-1} \text{ cm}^{-1}$), as reported previously (31). Assays were typically conducted in 50 mM MOPS (pH 7.4) with 0.1 mM EDTA, and the sequential addition of NADH (100–200 μM), Rd (2–10 μM), NROR (0.1 μM for O₂ reduction and 0.2 μM for NO reduction), and FDP (from 50 nM to 1 μM for O₂ reduction and from 9 to 17 μM for NO reduction) (concentrations on an FMN or diiron basis). Small volumes of aqueous O₂- or NO-saturated stock solutions were injected into the initially anaerobic assay solutions to initiate the reactions. Alternatively, gaseous air or 0.1 atm of NO was introduced into the headspace of the initially anaerobic UV-vis cuvette containing the assay solutions, which were stirred to maximize equilibration with the headspace gas.

The production of N₂O was monitored by FTIR spectroscopy with the $\nu(\text{N}-\text{N})$ mode of N₂O at 2230 cm⁻¹, as previously reported (28). Briefly, protein solutions ranging from 1 to 2 mM were made anaerobic by prolonged purging with argon on a Schlenk line and reduced with 8 mM dithionite followed by removal of excess reduction agents with desalting spin columns (Zebra, Pierce) in a glovebox containing < 1 ppm O₂ (Vacuum Atmospheres Co.). A diethylamine NONOate (Cayman Chemical, Ann Arbor, MI) stock solution was prepared using an ϵ_{250} extinction coefficient of 6500 M⁻¹ cm⁻¹ in 0.01 M NaOH, and additions of aliquots to deoxymyoglobin were used to confirm the concentration of the NO produced. Soon after the addition of the NONOate stock aliquot to the reduced protein, a 30 μL droplet of sample was deposited on a CaF₂ window and sealed by dropping a second CaF₂ window to complete the FTIR liquid cell. The optical path length was controlled by a 100 μm Teflon

spacer. FTIR spectra were recorded at room temperature on a Bruker Tensor 27 instrument equipped with a liquid N₂-cooled MCT detector and purged with compressed air, dried, and depleted of CO₂ (Purge gas generator, puregas LLC). Sets of 100-scan accumulations were acquired at 4 cm⁻¹ resolution, until no further growth of the 2230 cm⁻¹ band was observed. The FTIR spectrum of a buffer blank was also recorded under the same conditions for background subtraction.

Preparation of NO Adducts. Deflavo-FDP was made anaerobic by prolonged purging with either argon or nitrogen gas on a Schlenk line before being transferred to an anaerobic glovebox. Fully reduced enzyme was obtained either by titration to achieve a slight stoichiometric excess of sodium dithionite or by addition of excess dithionite followed by removal of the reducing agent with desalting spin columns. Stoichiometric addition of NO to fully reduced protein was achieved via addition of small aliquots of NO-saturated solutions after the stock concentration had been determined by titration against deoxymyoglobin. Alternatively, NONOate was added to reduced protein solutions in Eppendorf tubes. In both cases, these additions were made just prior to the transfer of samples into EPR tubes, Raman capillaries, or FTIR cells. To prepare the NO adducts observed at high NO concentrations, the headspaces over reduced protein solutions were replaced with NO (¹⁴NO purchased from Airgas and treated with a 1 M KOH solution; ¹⁵NO and ¹⁵N¹⁸O from Aldrich) directly in UV-vis cuvettes, EPR tubes, or Raman capillaries. For FTIR measurements, the NO adducts were prepared in Eppendorf tubes before being immediately transferred to CaF₂ cells.

Molecular Spectroscopies. UV-vis absorption spectra were recorded on either Varian Cary 50 or Ocean Optics USB 2000 spectrophotometers in anaerobic UV-vis cuvettes, EPR tubes, Raman capillaries, or FTIR sandwiched cells.

EPR spectra were recorded with a Bruker E500 X-band EPR spectrometer equipped with a superX microwave bridge and a dual-mode cavity with a helium flow cryostat (ESR900, Oxford Instruments, Inc.). Quantitation of the EPR signals was performed under nonsaturating conditions by double integration and comparison with series of concentrations of Cu(II)EDTA and Fe(II)EDTA(NO) standards.

RR spectra were recorded using a custom McPherson 2061/207 spectrograph (set at 0.67 m with variable gratings) equipped with a liquid N₂-cooled CCD detector (LN-1100PB, Princeton Instruments). The 458 nm excitation laser was derived from an Ar laser (Innova 90, Coherent). A long-pass filter (RazorEdge, Semrock) was used to attenuate Rayleigh scattering. RR spectra were recorded at room temperature in a 90° scattering geometry on samples mounted on a reciprocating translation stage. To assess the photosensitivity of the NO adduct, rapid acquisitions with minimal laser power and continuous sample translation were compared with longer data acquisitions on static samples. Frequencies were calibrated relative to indene and aspirin standards and are accurate to $\pm 1 \text{ cm}^{-1}$. Polarization conditions were optimized using CCl₄ and indene. The integrity of the RR samples was confirmed by direct monitoring of their UV-vis absorption spectra in Raman capillaries before and after laser exposure. Typical enzyme concentrations for RR experiments were 1 mM.

FTIR photolysis experiments were conducted as described previously (27, 28). Approximately 15 μL of 1.2 mM protein solutions was loaded in FTIR cells with a path length of 15 μm . After the presence of the NO adduct had been confirmed by

UV-vis absorption spectroscopy, the FTIR cell was mounted to a closed-cycle cryogenic system (Displex and Omniplex, Advanced Research System) and placed inside the sample compartment of the FTIR instrument. The sample was kept in the dark while it was cooled to <30 K. FTIR spectra were recorded on a Perkin-Elmer System 2000 and a Bruker Tensor 27, both equipped with a liquid N_2 -cooled MCT detector. Sets of 1000-scan accumulations were acquired at 4 cm^{-1} resolution. Photolysis of the nitrosyl complexes was performed by continuous illumination of the sample directly in the FTIR sample chamber using a 50 W tungsten lamp after filtering out heat and NIR emissions. The complete reversibility of the photolysis processes described below was confirmed by reproduction of the same FTIR difference spectra after annealing the samples above 40 K.

RESULTS

Characterization of *Tm* FDP and Deflavo-FDP. Heterologous expression in *Escherichia coli* and purification of *Tm* FDP produce an enzyme only partially (20–30%) loaded with FMN (assuming one FMN per protein monomer constitutes 100% loading). The FMN loading can be increased to $\sim 50\%$ if the growth temperature of the *E. coli* culture is increased from 37

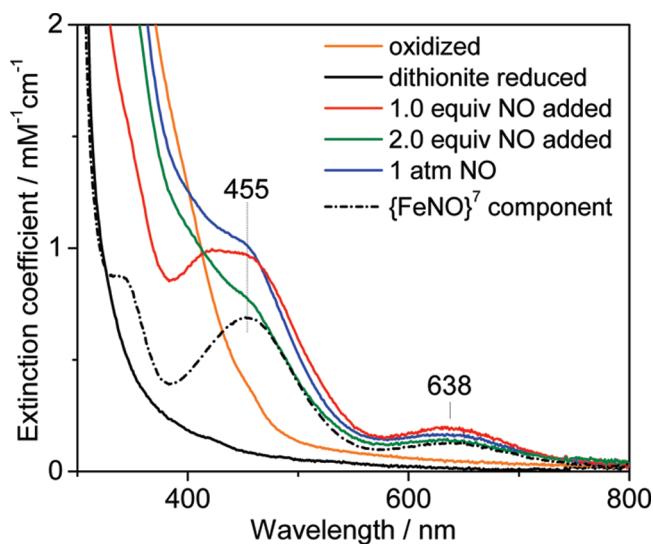


FIGURE 2: UV-vis absorption spectra of oxidized (orange), dithionite-reduced (black), and reduced deflavo-FDP after addition of 1 equiv (red), 2 equiv (green), and 1 atm of NO (blue) at room temperature [protein concentration of $147\text{ }\mu\text{M}$ in 50 mM MOPS (pH 7.4); extinction coefficient per diiron site]. Also shown is the (1 atm of NO spectrum) – 0.65(oxidized spectrum) difference spectrum (black dashed line).

to $42\text{ }^{\circ}\text{C}$ at the time of induction of FDP overexpression (31). Multiple preparations of *Tm* FDP contain 2.0 ± 0.2 Fe atoms per protein monomer irrespective of the FMN content. These observations are similar to those described in a previous report on heterologously expressed *Tm* FDP (29). O_2R and NOR activities of *Tm* FDP were measured via NADH consumption using the *Tm* redox protein components, NROR (encoding gene adjacent to that of FDP) and Rd (Scheme 1). The steady-state activity parameters k_{cat} and k_{cat}/K_M , determined from fitting to Michaelis–Menten plots (Figure S1 of the Supporting Information), are 4 s^{-1} and $2 \times 10^6\text{ M}^{-1}\text{ s}^{-1}$, respectively, for O_2R activity and 0.05 s^{-1} and $700\text{ M}^{-1}\text{ s}^{-1}$, respectively, for NOR activity. Neither activity is observed if any one of the protein components (FDP, NROR, or Rd) is omitted from the assay solutions. The relatively low NOR activity of *Tm* FDP prevents a reliable assessment of cooperativity, which, for some FDPs, is evident from the sigmoidal forms of the Michaelis–Menten plots (31).

Essentially complete removal of FMN from as-isolated *Tm* FDP is achieved by an acid wash (pH 2.5) of the protein bound to phenyl Sepharose prior to elution of deflavo-FDP at pH 7.3. The deflavo-FDP consistently retains 2 Fe atoms per protein monomer. As expected, the UV-vis absorption features of FMN are absent from the spectrum of the *Tm* deflavo-FDP (Figure S2 of the Supporting Information). The integrity of the diiron site in the absence of FMN is supported by the crystal structure of *Tm* FDP (PDB entry 1VME) which has no FMN bound and shows a diiron site structure and overall protein fold very similar to those observed in the crystal structure of *Mt* FDP (PDB entry 1YCF) (Figure 1 and Figure S3 of the Supporting Information). This structural equivalence has been confirmed by a crystal structure of the *Tm* deflavo-FDP prepared in our lab (A. Taylor, P. J. Hart, J. Caranto, and D. M. Kurtz, Jr., unpublished observation). As anticipated, the deflavo-FDP has no detectable multiturnover O_2R or NOR activity (Figure S2 of the Supporting Information), but the deflavo-FDP can be quantitatively reconstituted with FMN while retaining full iron occupancy. The refluvinated protein shows full restoration of O_2R and NOR activity (Figure S2 of the Supporting Information).

UV-Vis Spectral Characterization of the Reaction of Reduced Deflavo-FDP with NO. Reduction of deflavo-FDP with dithionite results in the loss of broad absorption features between 350 and 420 nm that originate from carboxylate and bridging oxo/hydroxo-to-iron(III) LMCT transitions (Figure 2), and presumably represents the diferrous deflavo-FDP. Addition of up to 1 equiv of NO to reduced deflavo-FDP produces a pale yellow color associated with absorption bands at 420, 455, and

Table 1: Spectroscopic Properties of Non-Heme Ferrous–Nitrosyl Complexes Containing O/N Ligands

{FeNO} ⁷ species	λ_{max} (nm) [ϵ ($\text{M}^{-1}\text{ cm}^{-1}$)] ^a	$\nu(\text{Fe}-\text{NO})$ ($\Delta^{15}\text{N}$) (cm^{-1})	$\delta(\text{Fe}-\text{N}-\text{O})$ ($\Delta^{15}\text{N}$) (cm^{-1})	$\nu(\text{N}-\text{O})$ ($\Delta^{15}\text{N}$) (cm^{-1})	ref
deflavo-FDP–(NO)	420, 455 (1000)	451 (–9)		not observed	this work
deflavo-FDP–(NO) ₂	455 (1000)	459 (–7)	444 (–8)	1749 (–30)	this work
wild-type R2–(NO) ₂	450 (760)	445 (–7)	434 (–9)	1742 (–29)	21, 23
D84E-R2–(NO) ₂	450 (1200)	454 (–8)	442 (–8)	1735 (–30)	23
hemerythrin–(NO)	408 (1000)	433 (–6)	421 (–6)	not observed	35
superoxide reductase–(NO)	475 (530)	475 (–7)		1721 (–31)	52
Fe(EDTA)–(NO)	434 (900)	496 (–4)	493 (–10)	1776 (–37)	this work, 40, 53
[Fe ₂ (NO) ₂ (μ -XDK)(μ -O ₂ CPh)(ImH) ₂ (O ₂ CPh)(MeOH)]	450 (1000)	nr ^b	nr ^b	nr ^b	23
Fe ₂ (NO) ₂ (Et-HPTB)(O ₂ CPh)(BF ₄) ₂	nr ^{b,c}	nr ^b	nr ^b	1785	47

^aPer iron. ^bNot reported. ^cObscured by ligand absorptions.

638 nm (Figure 2 and Figure S4 of the Supporting Information). These absorption features are characteristic of nitrosyl-to-iron LMCT transitions of non-heme $\{\text{FeNO}\}^7$ complexes with O/N ligands (Table 1) (21–23, 32–36). At 1 equiv of NO per diiron site, the 420/455 nm absorption corresponds to an $\epsilon_{420/455}$ of $\sim 1000 \text{ M}^{-1} \text{ cm}^{-1}$ which is a good match for non-heme $\{\text{FeNO}\}^7$ species in proteins and the synthetic model (Table 1). The high absorbance at 420/455 nm reached with 1 equiv of NO also suggests that the diiron(II) site binds NO with high affinity. We refer to this NO–diiron complex as deflavo-FDP–(NO). Further addition of NO, up to 2 equiv, results in a significant loss of the nitrosyl-to-iron LMCT bands in favor of absorption increases below 420 nm (Figure 2 and Figure S4 of the Supporting Information). These absorption changes suggest that the addition of >1 equiv of NO per diiron site promotes the formation of oxidized, presumably diferric, deflavo-FDP. However, this conversion is incomplete, and further NO addition results in increased absorptions at 455 and 638 nm (Figure 2 and Figure S4 of the Supporting Information). These rising absorption features at high NO concentrations are assigned to a deflavo-FDP–(NO)₂ complex that forms in parallel with oxidized deflavo-FDP (see below).

The NO adducts that form at high versus low NO:protein ratios can be distinguished by their sensitivity toward dithionite. Specifically, when the deflavo-FDP–(NO) complex is exposed to a 2-fold molar excess of dithionite at room temperature, the nitrosyl-to-iron LMCT transitions are bleached in a monotonous fashion with a slow apparent $t_{1/2}$ of ~ 15 min (Figure S5A of the Supporting Information). In contrast, the 455 nm absorption due to the deflavo-FDP–(NO)₂ complex formed with excess NO decays upon exposure to dithionite within the manual mixing time (Figure S5B of the Supporting Information). This rapid bleaching is accompanied by the slower reduction of the oxidized diiron sites; the residual absorption that decays at an even slower rate is likely to correspond to a small population of mixed-valent $\text{Fe}^{\text{III}}\text{Fe}^{\text{II}}$ sites (Figure S5B of the Supporting Information). This interpretation is supported by the UV–vis spectral changes observed for the reaction of 2 equiv of dithionite with oxidized deflavo-FDP (Figure S5C of the Supporting Information). In this experiment, the spectrum obtained immediately after mixing is distinct from that of the oxidized deflavo-FDP, and the relative absorbance loss near 400 nm and gain at ~ 500 nm can be assigned to mixed-valent diiron contributions; subsequent traces show a slow bleaching of these visible absorptions that is equivalent to the later changes observed during dithionite reduction of the deflavo-FDP–(NO)₂ complex/oxidized deflavo-FDP mixture. Taken together, these data suggest that the bleaching of the deflavo-FDP–(NO) complex by dithionite reflects the slow NO off rate from the mononitrosyl complex as dithionite scavenges free NO from solution. The faster reaction of the deflavo-FDP–(NO)₂ complex with dithionite could reflect either a faster NO off rate or super-reduction of the diiron–dinitrosyl complex.² The fraction of oxidized deflavo-FDP present in the

mixture produced by exposure of the reduced protein to a high level of NO is re-reduced slowly by dithionite with formation of mixed-valent and diferrous states.

The picture that emerges from these experiments is that the deflavo-FDP diferrous site binds one NO molecule with relatively high affinity before further reaction with excess NO to produce a mixture of oxidized deflavo-FDP and unreactive $\{\text{FeNO}\}^7$ centers. Presuming the as-isolated spectrum is equivalent to the post-NO-treated oxidized spectrum, we subtracted its contribution to the absorption spectra; the remaining spectra correspond to the fraction of non-heme $\{\text{FeNO}\}^7$ complexes with absorption bands at 455 and 638 nm (Figure 2). Using this analysis, the fraction of oxidized protein resulting from the excess NO treatment was consistently reproducible for individual deflavo-FDP preparations, typically ranging from 60 to 70%, but reaching only 40% for one of the preparations (Figure S6 of the Supporting Information). The origin of this variability is currently unclear. The remaining absorbance at 455 nm corresponds to a molar extinction coefficient of $\sim 1000 \text{ M}^{-1} \text{ cm}^{-1}$ per iron. This value is again in good agreement with those of other non-heme $\{\text{FeNO}\}^7$ complexes (Table 1) and suggests that the diiron sites that do not proceed to the diiron(III) state instead form stable diferrous–dinitrosyl $[\{\text{FeNO}\}^7]_2$ clusters, as previously observed with reduced R2 exposed to excess NO (21, 23).

FTIR Evidence of N_2O Production. Consistent with the UV–vis absorption analysis, FTIR spectroscopy shows production of N_2O from the reaction of excess NO with reduced deflavo-FDP. Specifically, we detect the N–N stretching mode of N_2O at 2330 cm^{-1} in the FTIR spectra of deflavo-FDP samples and compare these measurements with data for myoglobin and terminal oxidases as negative and positive controls, respectively (Figure S7 of the Supporting Information). The intensity of the FTIR band at 2330 cm^{-1} upon completion of the reaction reveals that ~ 0.7 equiv of N_2O is formed per deflavo-FDP diiron site, which closely matches the estimated fraction of oxidized diferric deflavo-FDP from UV–vis absorption spectroscopy. A comparable FTIR experiment with fully reduced refluvinated FDP exposed to excess NO from NONOate shows ~ 2.0 equiv of N_2O produced per FDP diiron site (Figure S7 of the Supporting Information), which confirms that all reducing equivalents are used to produce N_2O .

EPR Characterization of the Reaction of Reduced Deflavo-FDP with NO. As established earlier for native FDPs (3, 30, 37), the oxidized diiron site of deflavo-FDP is EPR silent since a bridging solvent and carboxylate ligands promote antiferromagnetic coupling of the two non-heme iron(III) ions. The dithionite-reduced deflavo-FDP is also EPR silent, as expected for a fully reduced diiron(II) site with no evidence of formation of a mixed-valent $\text{Fe}(\text{II})\cdot\text{Fe}(\text{III})$ cluster, and consistent with previous redox titrations of FDPs (30, 37). Addition of 1 equiv of NO results in the appearance of a $g \sim 2$ broad axial EPR signal which we assign to an $S = 1/2$ diiron–mononitrosyl species produced by antiferromagnetic coupling of an $S = 2$ $\text{Fe}(\text{II})$ to an $S = 3/2$ $\{\text{FeNO}\}^7$ species (Figure 3). This EPR spectrum is reminiscent of the axial signals of hemerythrin–NO adducts with g_{\parallel} and g_{\perp} near 2.8 and 1.8, respectively (35, 38), although the anisotropic components of deflavo-FDP(NO) are more difficult to pinpoint because the splitting is small and the g strain on both g_{\parallel} and g_{\perp} is relatively large. Double integrations of the EPR signal of the deflavo-FDP–(NO) complex against $\text{Cu}(\text{II})\text{EDTA}$ standards indicate that the axial $g \sim 2$ signal represents 0.75 spin per diiron site. This deviation from stoichiometry is easily

²To the best of our knowledge, $[S = 3/2 \{\text{FeNO}\}^7]/[\text{FeN}(\text{H})\text{O}]^8$ reduction potentials have not been reported. The reduction potentials for NO/NO^- and NO/HNO couples are -0.8 and -1.7 V, respectively. In iron porphyrins (54), heme proteins (55), and octahedral non-heme iron complexes (56), $\{\text{FeNO}\}^7$ species are $S = 1/2$ systems with reduction potentials between ca. -0.6 and -1.4 V. While these reduction potentials suggest that those of $S = 3/2 \{\text{FeNO}\}^7$ species are inaccessible to dithionite, the $\{\text{FeNO}\}^6$ species nitroprusside ion, $[\text{Fe}(\text{CN})_5(\text{NO})]^{2-}$, was recently shown to be reducible to the $\{\text{FeN}(\text{H})\text{O}\}^8$ species by 2 equiv of dithionite in aqueous solution at pH 10 (57).

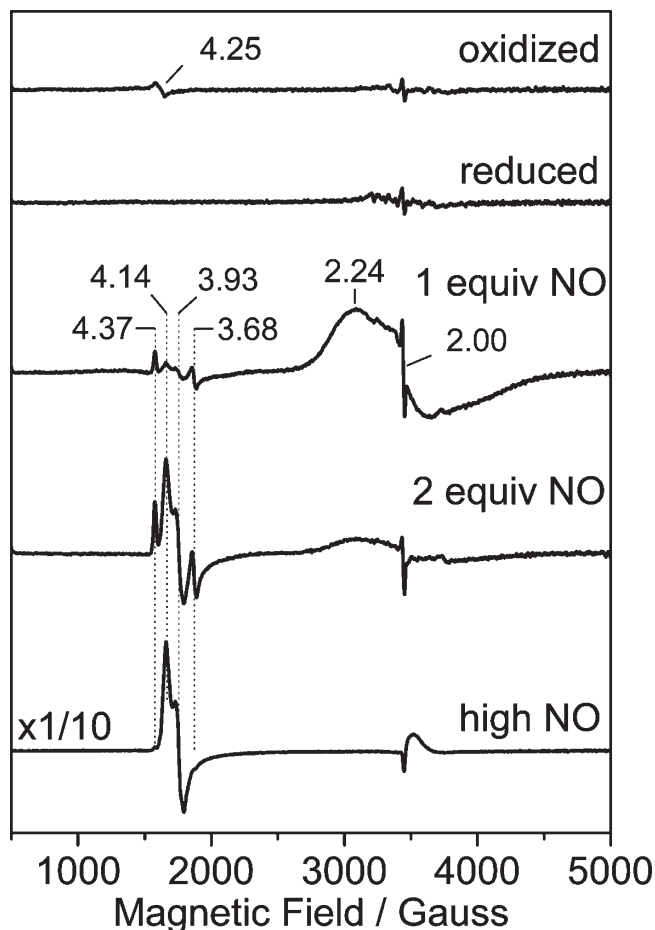


FIGURE 3: EPR spectra of oxidized deflavo-FDP, dithionite-reduced deflavo-FDP, and reduced deflavo-FDP after the addition of 1 equiv, 2 equiv, and 0.05 atm of NO headspace at 4.2 K. Conditions: protein concentration of 100 μ M in 50 mM MOPS (pH 7.4), microwave frequency of 9.66 GHz, microwave power of 2 mW, and modulation amplitude of 10 G.

explained if one accounts for some dissociation of NO from the deflavo-FDP-(NO) complex prior to the EPR tubes being frozen since the complex is prepared without an excess of NO; a slight overshoot in the NO addition, > 1 equiv, will also lower the deflavo-FDP-(NO) complex content to produce a fraction of diferric deflavo-FDP. As expected from the UV-vis experiments, the $g \sim 2$ EPR signal from the diiron-mononitrosyl complex disappears upon addition of 2 equiv of NO, concomitant with the appearance of new $g \sim 4$ EPR resonances (Figure 3).

These $g \sim 4$ EPR features are consistent with rhombic EPR signatures from $S = 3/2$ $\{\text{FeNO}\}^7$ species (39, 40). Comparing double integrations of these signals with those of Fe(II)EDTA-(NO) standards shows that less than 3% of the total iron content contributes to these regions of the EPR spectra in deflavo-FDP samples treated with 2 equiv of NO, but that this value increases to $\sim 30\%$ of the total iron when the free NO concentration is increased to 100 μ M with an 0.05 atm NO(g) headspace (Figure 3). Further increases in free NO concentration do not affect the intensity of the $g \sim 4$ signals (data not shown). The multiplicity of $g \sim 4$ resonances is readily assigned to two distinct $S = 3/2$ $\{\text{FeNO}\}^7$ species, a more rhombic one with g values of 4.37, 3.68, and 2.00 and another with g values of 4.14, 3.93, and 2.0 (Figure 3). While the more rhombic signal represents a minor species at all NO concentrations, the more axial species becomes prominent at the higher NO concentration. The quantitation

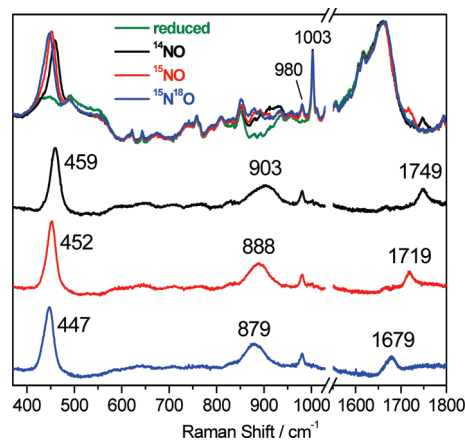


FIGURE 4: Room-temperature RR spectra of reduced deflavo-FDP [protein concentration of ~ 1 mM in 50 mM MOPS (pH 7.4)] before (green) and after exposure to excess ^{14}NO (top black), ^{15}NO (top red), and $^{15}\text{N}^{18}\text{O}$ (top blue). The three bottom spectra are “NO complexes” minus “reduced” difference spectra color-coded as for the top spectra. The spectral subtractions were normalized on the 1003 cm^{-1} band from Phe; the sharp 980 cm^{-1} band originates from the sulfate byproduct of dithionite oxidation.

of the $g \sim 4$ signals matches well with the $\sim 30\%$ of diferrous-dinitrosyl $[\{\text{FeNO}\}^7]_2$ sites estimated from the UV-vis analysis. The EPR data, thus, imply that the remaining 30% of deflavo-FDP diiron sites form $\{\text{FeNO}\}^7$ centers that are magnetically uncoupled. This observation is in striking contrast with the magnetically coupled, EPR-silent diferrous-dinitrosyl $[\{\text{FeNO}\}^7]_2$ sites of the R2-(NO)₂ complex (21, 23).

RR and FTIR Characterization of Reduced Deflavo-FDP-NO Complexes. The deflavo-FDP-(NO)₂ complex resulting from the reaction of reduced protein with excess NO is sufficiently stable to allow extended acquisition times for optimal RR spectral characterization. As expected, the RR spectra obtained with 458 nm laser excitation revealed enhancement of vibrational modes characteristic of the $\{\text{FeNO}\}^7$ unit (Figure 4 and Table 1). A band at 459 cm^{-1} that downshifts to 452 (-7) and 447 (-12) cm^{-1} with ^{15}NO and $^{15}\text{N}^{18}\text{O}$, respectively, is assigned to the $\nu(\text{Fe}-\text{NO})$ mode. In the high-frequency region, a band at 1749 cm^{-1} downshifts to 1719 (-30) and 1679 (-70) cm^{-1} with ^{15}NO and $^{15}\text{N}^{18}\text{O}$, respectively (Figure 4), and is readily assigned to the $\nu(\text{N}-\text{O})$ mode. In addition to these two Fe-N-O vibrations, another isotope-sensitive RR band is observed at 903 cm^{-1} and shifts to 888 (-15) and 879 (-24) cm^{-1} with ^{15}NO and $^{15}\text{N}^{18}\text{O}$, respectively. Comparable RR signals in the 900 cm^{-1} region for the NO adduct of R2 were assigned to a combination of bending and stretching Fe-N-O modes (23). An equivalent RR band and isotope dependence are observed for the mononuclear complex, Fe(II)EDTA-(NO) (Figure S8 of the Supporting Information), which rules out some alternative assignments, such as a bound hyponitrite (41), for this midfrequency vibration. All of these assignments are consistent with those listed in Table 1 for $\{\text{FeNO}\}^7$ units in other proteins and synthetic complexes, including the deduced Fe-N-O bending/stretching combination modes.

The $[\{\text{FeNO}\}^7]_2$ complex of deflavo-FDP can also be characterized by light-induced FTIR difference spectroscopy at low temperatures. The “dark” minus “illuminated” difference spectra obtained at 30 K show a single $\nu(\text{N}-\text{O})$ at 1751 cm^{-1} that shifts to 1721 (-30) cm^{-1} with ^{15}NO (Figure 5). These frequencies are in good agreement with those observed in the RR spectra and

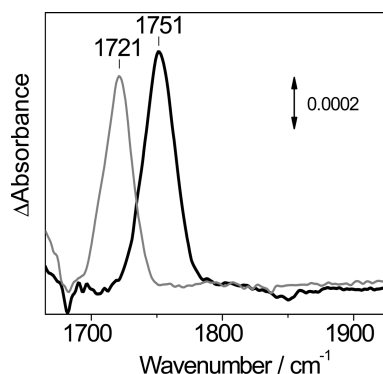


FIGURE 5: FTIR difference spectra (dark minus illuminated) of deflavo-FDP-(^{14}NO)₂ (black) and deflavo-FDP-($^{15}\text{N O}$)₂ (gray) complexes obtained at < 30 K (protein concentration of ~1.2 mM).

support the notion that the two {FeNO}⁷ units experience similar environments within the protein matrix. Nitrosyl ligands, when photodissociated from metal centers at cryogenic temperatures, typically remain as free NO molecules trapped within the protein pocket and typically exhibit very weak $\nu(\text{N-O})$ modes between 1850 and 1860 cm⁻¹ (23, 28, 42). Such vibrations should appear as negative band(s) in the FTIR difference spectra, but so far, we have not detected such signals in a reproducible fashion in the light-induced difference spectra of the deflavo-FDP-(NO)₂ complex. The empty FMN-binding site may provide a more expansive pocket with multiple docking sites for the dissociated NO, which may broaden these signals beyond detection.

The mononitrosyl deflavo-FDP-(NO) complex forms without appreciable fractions of the dinitrosyl complex only when using ≤ 1 equiv of NO per diiron site. Under these conditions, significant dissociation and degassing of free NO can take place in RR capillaries. Nevertheless, RR spectra recorded with an acquisition time of a few minutes reveal vibrational modes similar to those of the [{FeNO}⁷]₂ complex, but at lower energy (Figure 6). A broad RR band centered at 451 cm⁻¹ downshifts to 442 (-9) and 436 (-15) cm⁻¹ with ^{15}NO and $^{15}\text{N}^{18}\text{O}$, respectively.³ In addition, changes in half-widths and bandshapes with different NO isotopes in the deflavo-FDP-(NO) complex suggest that this broad band may be composed of more than one unresolved component and may reflect overlapped bending and stretching modes of the Fe-N-O unit. Because of the low signal-to-noise ratio of these RR spectra, no other vibrational modes could be clearly identified. As expected, additions of excess NO to the mononitrosyl complexes produce RR spectra equivalent to those of the deflavo-FDP-(NO)₂ complex (data not shown). Low-temperature FTIR photolysis experiments conducted to further characterize the deflavo-FDP-(NO) complex were unsuccessful.

DISCUSSION

The heterologously expressed *Tm* FDP has a full diiron site but only partial FMN occupancy. We found that the as-isolated protein has a high O₂R activity relative to its NOR activity. The O₂R activity is consistent with its upregulation in *T. maritima* exposed to oxidative conditions (29). Nevertheless, the relatively low NOR activity of the heterologously expressed *Tm* FDP is still significantly above background. Whether this NOR activity is physiologically relevant in *T. maritima* remains to be determined,

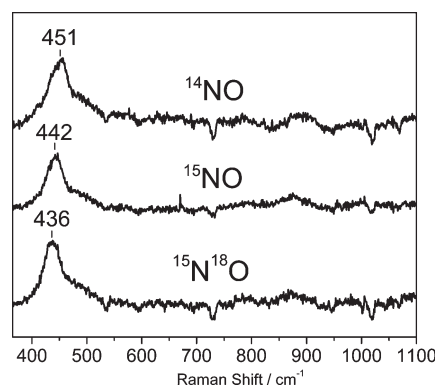


FIGURE 6: Room-temperature RR difference spectra ("NO complexes" minus "reduced protein") of the deflavo-FDP-(NO) complex formed with ^{14}NO (top), ^{15}NO (middle), and $^{15}\text{N}^{18}\text{O}$ (bottom) [protein concentration of ~1 mM in 50 mM MOPS (pH 7.4)].

but in other organisms, FDPs appear to confer both oxidative and nitrosative stress protection in vivo (43, 44).

In an attempt to distinguish between NOR mechanisms of FDPs described in the introductory section, we prepared *Tm* deflavo-FDP and characterized its reaction with NO. In agreement with the deposited X-ray crystal structure (and our own), our results demonstrate that the FMN cofactor can be removed from *Tm* FDP without irreversible disruption of the protein structure and, specifically, that the diiron site remains intact in the FMN-free protein. As expected, the FMN-free FDP is catalytically inactive but can be readily and quantitatively reconstituted with FMN, while retaining full iron occupancy. The refluvinated protein regains O₂R and NOR activities indistinguishable from those of the initially isolated protein on an FMN basis.

Stoichiometric addition of one NO per diiron site to reduced deflavo-FDP results in the formation of a stable deflavo-FDP-(NO) complex. The UV-vis absorption spectrum of this complex, with bands at 420, 455, and 638 nm, is characteristic of non-heme {FeNO}⁷ complexes containing oxygen and nitrogen ligands. The calculated extinction coefficient of the chromophoric species ($\epsilon_{420/455} \sim 1000 \text{ mM}^{-1} \text{ cm}^{-1}$) is in good agreement with values reported for other proteins and synthetic {FeNO}⁷ complexes (Table 1). Such {FeNO}⁷ complexes are best described as $S = 3/2$ species with a high-spin iron(III) ($S = 5/2$) antiferromagnetically coupled to an NO⁻ ($S = 1$) and show characteristic $g \sim 4$ EPR signals (43, 44). In the deflavo-FDP-(NO) complex, antiferromagnetic coupling between the $S = 3/2$ {FeNO}⁷ and the second $S = 2$ iron(II) produces an $S = 1/2$ [$\text{Fe}^{\text{II}} \cdot \{\text{FeNO}\}^7$] species that exhibits a broad $g \sim 2$ signal, as previously observed in the NO adduct of hemerythrin (43, 44). The double integration of this EPR signal suggests that the stoichiometric addition of NO nearly quantitatively converts the diiron(II) to [$\text{Fe}^{\text{II}} \cdot \{\text{FeNO}\}^7$] sites. To the best of our knowledge, this is the first example of a diferrous-mononitrosyl complex formed in a diiron(II) protein or synthetic complex where the two metals share the same ligand set.

The near-stoichiometric formation of the diferrous-mononitrosyl complex implies that, at least in deflavo-FDP, the first NO molecule binds with an affinity higher than that of the second NO. This order of NO affinity seems to be in conflict with the cooperativity in NO binding inferred from the sigmoidal Michaelis-Menten plots for NOR activities of some other FDPs (3, 31, 45). The relatively low NOR activity of flavinated *Tm* FDP may reflect a lack of cooperativity in NO binding.

³The impact of ^{18}O labeling on the observed frequency may reflect the contribution from Fe-N-O bending and/or one-body stretching motions of the NO group with regard to the iron.

Scheme 3



Relative NOR versus O_2R activities are also variable among FDPs for unknown reasons (1–6, 46).

Further addition of NO of up to 2 equiv and beyond results in a change in the UV–vis absorption spectrum and the loss of the broad $g = 2$ EPR signal, consistent with NO reacting with the diferrous–mononitrosyl site. The product of this reaction is not homogeneous: up to 70% of the diiron sites are catalytically competent and produce N_2O , as revealed by FTIR, while the remaining diiron sites form magnetically uncoupled $\{\text{FeNO}\}^7$ $S = 3/2$ species with characteristic $g \sim 4$ EPR signatures. Quantitative analyses of the UV–vis, FTIR, and EPR data all support these relative proportions for a given deflavo-FDP preparation, even though some variability in proportions of the two diiron products was observed from preparation to preparation.

The lack of magnetic coupling between the two $\{\text{FeNO}\}^7$ centers of deflavo-FDP(NO)₂ requires a major disruption of the efficient exchange coupling pathway provided by the oxo/hydroxo solvent bridge between the iron centers in the $[\text{Fe}^{\text{III}}\cdot\text{Fe}^{\text{III}}]$ site, in mixed-valent $[\text{Fe}^{\text{II}}\cdot\text{Fe}^{\text{III}}]$ diiron sites, and in the $[\text{Fe}^{\text{II}}\cdot\{\text{FeNO}\}^7]$ diiron–mononitrosyl complex (3, 30, 37). Presumably, the solvent bridge is lost upon formation of the diferrous–dinitrosyl complex, while the bridging Asp carboxylate present in both reduced and oxidized FDP diiron sites may or may not remain. To the best of our knowledge, there has been no report of synthetic analogues containing a carboxylate-bridged diiron site without at least one other supporting bridge. The only well-characterized, carboxylate-bridged, non-heme, O/N-ligated diferrous–dinitrosyl synthetic complex, $\text{Fe}_2(\text{NO})_2(\text{Et-HPTB})(\text{O}_2\text{CPh})(\text{BF}_4)_2$, includes an additional bridging alkoxo ligand (47). This complex is EPR silent due to antiferromagnetic coupling between the two $\{\text{FeNO}\}^7$ centers (47). In the case of the diferrous–dinitrosyl adduct of ribonucleotide reductase R2 protein, the antiferromagnetic coupling between the two irons (and EPR silent character) may be due to the presence of both bidentate and monodentate carboxylate bridges, as observed in the diferrous R2 protein (15). Dinuclear Mn(II) sites in both proteins and synthetic complexes containing a bidentate carboxylate as the only bridging ligand have reportedly shown no evidence of magnetic exchange coupling (48, 49). A single bridging carboxylate with anti-syn configuration can accommodate a metal–metal distance of >6.3 Å (50, 51), and the two $\{\text{FeNO}\}^7$ units could move further apart if the bridging carboxylate group adopts a nonbridging conformation. We view these data as evidence of conformational flexibility at the diiron site because uncoupling of the two irons at the active site is fully reversible and is not associated with iron loss. Indeed, the $[\{\text{FeNO}\}^7]_2$ species can be reoxidized after exchanging the sample headspace, first with Ar and then with O_2 , re-reduced, and re-exposed to NO to regenerate the same fraction of $[\{\text{FeNO}\}^7]_2$ species, with no loss of iron (data not shown). Similarly, two consecutive redox cyclings of the deflavo-FDP-(NO)₂ complex do not decrease the steady-state O_2R or NOR activity observed after FMN addition.

The vibrational characterization of uncoupled $[\{\text{FeNO}\}^7]_2$ reveals a single set of Fe–N–O vibrations, suggesting that the individual $\{\text{FeNO}\}^7$ units adopt equivalent configurations. The Fe–N–O vibrations of the deflavo-FDP-(NO)₂ complex are similar to those observed previously in the R2-(NO)₂ com-

plex (23), which is not unexpected because the endogenous iron ligands are comparable in both proteins. Our vibrational characterization of the deflavo-FDP-(NO) complex is less complete than for the dinitrosyl complex, but the $\nu(\text{Fe–NO})$ mode is only ~ 8 cm^{-1} lower than in the $[\{\text{FeNO}\}^7]_2$ complex.

The reactions of reduced deflavo-FDP with NO based on our results are summarized in Scheme 3. Reduction of NO to N_2O by the reduced diiron site in the absence of FMN (pathway A in Scheme 3) is consistent with the hyponitrite mechanism in Scheme 2. While Scheme 2, as suggested by the computational study by Siegbahn and co-workers (25), indicates that the second NO reacts with the $\{\text{FeNO}\}^7$ species rather than the second iron(II), a magnetically coupled diferrous–dinitrosyl complex could be a transient intermediate both in pathway A and in the hyponitrite mechanism. Thus, super-reduction of $\{\text{FeNO}\}^7$ units to nitroxyl $\{\text{FeN}(\text{H})\text{O}\}^8$ species does not represent an absolute requisite step in the NOR reaction pathway in FDPs. The parallel pathway B in Scheme 3 leading to a stable magnetically uncoupled diferrous–dinitrosyl intermediate may be prevented in the flavinated enzyme via steric constraints. Alternatively, turnover of an $[\{\text{FeNO}\}^7]_2$ complex in FDP may require reduction by the proximal FMN cofactor, as proposed in the “super-reduction” mechanism (Scheme 2) (5, 11). Uncoupling of the two $\{\text{FeNO}\}^7$ units may also permit a reaction pathway in the flavinated enzyme where each iron center functions independently to form mononuclear hyponitrite complexes, thereby maximizing scavenging efficiency under high-NO stress conditions. The results of this study provide a clear framework for further investigation of this unique family of enzymes.

ACKNOWLEDGMENT

We thank Drs. Adeniki Otoikhian and Ninian Blackburn for help with ICP-OES and Dr. James Whittaker for the use of his helium cryostat.

SUPPORTING INFORMATION AVAILABLE

O_2R and NOR activity assays of as-isolated and deflavo-FDPs; UV–vis absorption spectra of as-isolated, deflavo, and re-flavinated *Tm* FDPs; superposition of *Mt* FDP and *Tm* FDP protein backbones; UV–vis titrations of reduced deflavo-FDP with NO; UV–vis monitoring of the reaction of dithionite with the deflavo-FDP-(NO) complex, the deflavo-FDP-(NO)₂ complex, and oxidized deflavo-FDP; FTIR monitoring of N_2O production; and RR spectra of $\text{Fe}^{\text{II}}(\text{EDTA})\text{NO}$. This material is available free of charge via the Internet at <http://pubs.acs.org>.

REFERENCES

- Gardner, A. M., Helmick, R. A., and Gardner, P. R. (2002) Flavorubredoxin, an inducible catalyst for nitric oxide reduction and detoxification in *Escherichia coli*. *J. Biol. Chem.* 277, 8172–8177.
- Gomes, C. M., Giuffre, A., Forte, E., Vicente, J. B., Saraiva, L. M., Brunori, M., and Teixeira, M. (2002) A novel type of nitric-oxide reductase. *Escherichia coli* flavorubredoxin. *J. Biol. Chem.* 277, 25273–25276.
- Silaghi-Dumitrescu, R., Coulter, E. D., Das, A., Ljungdahl, L. G., Jameson, G. N., Huynh, B. H., and Kurtz, D. M., Jr. (2003) A flavodiiron protein and high molecular weight rubredoxin from *Moorella thermoacetica* with nitric oxide reductase activity. *Biochemistry* 42, 2806–2815.
- Saraiva, L. M., Vicente, J. B., and Teixeira, M. (2004) The role of the flavodiiron proteins in microbial nitric oxide detoxification. *Adv. Microb. Physiol.* 49, 77–129.
- Kurtz, D. M. J. (2007) Flavo-diiron enzymes: Nitric oxide or dioxygen reductases? *Dalton Trans.*, 4115–4121.
- Di Matteo, A., Scandurra, F. M., Testa, F., Forte, E., Sarti, P., Brunori, M., and Giuffre, A. (2008) The O_2 -scavenging flavodiiron

- protein in the human parasite *Giardia intestinalis*. *J. Biol. Chem.* 283, 4061–4068.
7. Wasser, I. M., de Vries, S., Moënné-Loccoz, P., Schroder, I., and Karlin, K. D. (2002) Nitric oxide in biological denitrification: Fe/Cu metalloenzyme and metal complex NO_x redox chemistry. *Chem. Rev.* 102, 1201–1234.
 8. Moënné-Loccoz, P. (2007) Spectroscopic characterization of heme iron-nitrosyl species and their role in NO reductase mechanisms in diiron proteins. *Nat. Prod. Rep.* 24, 610–620.
 9. Watmough, N. J., Field, S. J., Hughes, R. J., and Richardson, D. J. (2009) The bacterial respiratory nitric oxide reductase. *Biochem. Soc. Trans.* 37, 392–399.
 10. Frazao, C., Silva, G., Gomes, C. M., Matias, P., Coelho, R., Sieker, L., Macedo, S., Liu, M. Y., Oliveira, S., Teixeira, M., Xavier, A. V., Rodrigues-Pousada, C., Carrondo, M. A., and Le Gall, J. (2000) Structure of a dioxygen reduction enzyme from *Desulfovibrio gigas*. *Nat. Struct. Biol.* 7, 1041–1045.
 11. Silaghi-Dumitrescu, R., Kurtz, D. M., Jr., Ljungdahl, L. G., and Lanzilotta, W. N. (2005) X-ray crystal structures of *Moorella thermoacetica* FprA. Novel diiron site structure and mechanistic insights into a scavenging nitric oxide reductase. *Biochemistry* 44, 6492–6501.
 12. Nordlund, P., Sjöberg, B.-M., and Eklund, H. (1990) Three-dimensional structure of the free radical protein of ribonucleotide reductase. *Nature* 345, 593–598.
 13. Voegtli, W. C., Khidekel, N., Baldwin, J., Ley, B. A., Bollinger, J. M., and Rosenzweig, A. C. (2000) Crystal structure of the ribonucleotide reductase R2 mutant that accumulates a μ -1,2-peroxodiiron(III) intermediate during oxygen activation. *J. Am. Chem. Soc.* 122, 3255–3261.
 14. Baldwin, J., Voegtli, W. C., Khidekel, N., Moënné-Loccoz, P., Krebs, C., Pereira, A. S., Ley, B. A., Huynh, B. H., Loehr, T. M., Riggs-Gelasco, P. J., Rosenzweig, A. C., and Bollinger, J. M., Jr. (2001) Rational reprogramming of the R2 subunit of *Escherichia coli* ribonucleotide reductase into a self-hydroxylating monooxygenase. *J. Am. Chem. Soc.* 123, 7017–7030.
 15. Voegtli, W. C., Sommerhalter, M., Saleh, L., Baldwin, J., Bollinger, J. M., Jr., and Rosenzweig, A. C. (2003) Variable coordination geometries at the diiron(II) active site of ribonucleotide reductase R2. *J. Am. Chem. Soc.* 125, 15822–15830.
 16. Rosenzweig, A. C., Frederick, C. A., Lippard, S. J., and Nordlund, P. (1993) Crystal structure of a bacterial non-heme iron hydroxylase that catalyzes the biological oxidation of methane. *Nature* 366, 537–543.
 17. Rosenzweig, A. C., Nordlund, P., Takahara, P. M., Frederick, C. A., and Lippard, S. J. (1995) Geometry of the soluble methane monooxygenase catalytic diiron center in two oxidation states. *Chem. Biol.* 2, 409–418.
 18. Whittington, D. A., and Lippard, S. J. (2001) Crystal structures of the soluble methane monooxygenase hydroxylase from *Methylococcus capsulatus* (Bath) demonstrating geometrical variability at the dinuclear iron active site. *J. Am. Chem. Soc.* 123, 827–838.
 19. Lindqvist, Y., Huang, W., Schneider, G., and Shanklin, J. (1996) Crystal structure of Δ 9-stearoyl-acyl carrier protein desaturase from castor seed and its relationship to other di-iron proteins. *EMBO J.* 15, 4081–4092.
 20. Moche, M., Shanklin, J., Ghoshal, A., and Lindqvist, Y. (2003) Azide and acetate complexes plus two iron-depleted crystal structures of the di-iron enzyme Δ 9-stearoyl-acyl carrier protein desaturase. Implications for oxygen activation and catalytic intermediates. *J. Biol. Chem.* 278, 25072–25080.
 21. Haskin, C. J., Ravi, N., Lynch, J. B., Münck, E., and Que, L., Jr. (1995) Reaction of NO with the reduced R2 protein of ribonucleotide reductase from *Escherichia coli*. *Biochemistry* 34, 11090–11098.
 22. Coufal, D. E., Tavares, P., Pereira, A. S., Huynh, B. H., and Lippard, S. J. (1999) Reactions of nitric oxide with the reduced non-heme diiron center of the soluble methane monooxygenase hydroxylase. *Biochemistry* 38, 4504–4513.
 23. Lu, S., Libby, E., Saleh, L., Xing, G., Bollinger, J. M., Jr., and Moënné-Loccoz, P. (2004) Characterization of NO adducts of the diiron center in protein R2 of *Escherichia coli* ribonucleotide reductase and site-directed variants. Implications for the O₂-activation mechanism. *J. Biol. Inorg. Chem.* 9, 818–827.
 24. Enemark, J. H., and Feltham, R. D. (1974) Principles of structure, bonding, and reactivity for metal nitrosyl complexes. *Coord. Chem. Rev.* 13, 339–406.
 25. Blomberg, L. M., Blomberg, M. R., and Siegbahn, P. E. (2007) Theoretical study of the reduction of nitric oxide in an A-type flavoprotein. *J. Biol. Inorg. Chem.* 12, 79–89.
 26. Blomberg, M. L., Blomberg, M. R. A., and Siegbahn, P. E. M. (2006) A theoretical study of nitric oxide reductase activity in a ba₃-type heme-copper oxidase. *Biochim. Biophys. Acta* 1757, 31–46.
 27. Hayashi, T., Lin, I. J., Chen, Y., Fee, J. A., and Moënné-Loccoz, P. (2007) Fourier transform infrared characterization of a Cu₂-nitrosyl complex in cytochrome ba₃ from *Thermus thermophilus*: Relevance to NO reductase activity in heme-copper terminal oxidases. *J. Am. Chem. Soc.* 129, 14952–14958.
 28. Hayashi, T., Lin, M. T., Ganesan, K., Chen, Y., Fee, J. A., Gennis, R. B., and Moënné-Loccoz, P. (2009) Accommodation of two diatomic molecules in cytochrome bo: Insights into NO reductase activity in terminal oxidases. *Biochemistry* 48, 883–890.
 29. Le Fourn, C., Fardeau, M.-L., Ollivier, B., Lojou, E., and Dolla, A. (2008) The hyperthermophilic anaerobe *Thermotoga maritima* is able to cope with limited amount of oxygen: Insights into its defence strategies. *Environ. Microbiol.* 10, 1877–1887.
 30. Vicente, J. B., Testa, F., Mastronicola, D., Forte, E., Sarti, P., Teixeira, M., and Giuffrè, A. (2009) Redox properties of the oxygen-detoxifying flavodiiron protein from the human parasite *Giardia intestinalis*. *Arch. Biochem. Biophys.* 488, 9–13.
 31. Hillmann, F., Riebe, O., Fischer, R. J., Mot, A., Caranto, J. D., Kurtz, D. M., Jr., and Bahl, H. (2009) Reductive dioxygen scavenging by flavo-diiron proteins of *Clostridium acetobutylicum*. *FEBS Lett.* 583, 241–245.
 32. Arciero, D. M., Orville, A. M., and Lipscomb, J. D. (1985) [¹⁷O]Water and nitric oxide binding by protocatechuate 4,5-dioxygenase and catechol 2,3-dioxygenase. Evidence for binding of exogenous ligands to the active site Fe²⁺ of extradiol dioxygenases. *J. Biol. Chem.* 260, 14035–14044.
 33. Arciero, D. M., and Lipscomb, J. D. (1986) Binding of ¹⁷O-labeled substrate and inhibitors to protocatechuate 4,5-dioxygenase-nitrosyl complex. Evidence for direct substrate binding to the active site Fe²⁺ of extradiol dioxygenases. *J. Biol. Chem.* 261, 2170–2178.
 34. Nocek, J. M., Kurtz, D. M., Jr., Pickering, R. A., and Doyle, M. P. (1984) Oxidation of deoxyhemerythrin to semi-methemerythrin by nitrite. *J. Biol. Chem.* 259, 12334–12338.
 35. Nocek, J. M., Kurtz, D. M., Jr., Sage, J. T., Xia, Y. M., Debrunner, P., Shiemke, A. K., Sanders-Loehr, J., and Loehr, T. M. (1988) Nitric oxide adducts of the binuclear iron site of hemerythrin: Spectroscopy and reactivity. *Biochemistry* 27, 1014–1024.
 36. Chen, V. J., Orville, A. M., Harpel, M. R., Frolik, C. A., Surerus, K. K., Münck, E., and Lipscomb, J. D. (1989) Spectroscopic studies of isopenicillin N synthase. A mononuclear nonheme Fe²⁺ oxidase with metal coordination sites for small molecules and substrate. *J. Biol. Chem.* 264, 21677–21681.
 37. Vicente, J. B., and Teixeira, M. (2005) Redox and spectroscopic properties of the *Escherichia coli* nitric oxide-detoxifying system involving flavorubredoxin and its NADH-oxidizing redox partner. *J. Biol. Chem.* 280, 34599–34608.
 38. Nocek, J. M., Kurtz, D. M. J., Sage, J. T., Debrunner, P. G., Maroney, M. J., and Que, L. J. (1985) Nitric oxide adduct of the binuclear iron center in deoxyhemerythrin from *Phascolopsis gouldii*. Analogue of a putative intermediate in the oxygenation reaction. *J. Am. Chem. Soc.* 107, 3382–3384.
 39. Westre, T. E., Di Cicco, A., Filippini, A., Natoli, C. R., Hedman, B., Solomon, E. I., and Hodgson, K. O. (1994) Determination of the Fe-N-O angle in {FeNO}⁷ complexes using multiple-scattering EXAFS analysis by GNXAS. *J. Am. Chem. Soc.* 116, 6757–6768.
 40. Brown, C. A., Pavlosky, M. A., Westre, T. E., Zhang, Y., Hedman, B., Hodgson, K. O., and Solomon, E. I. (1995) Spectroscopic and theoretical description of the electronic structure of S = 3/2 iron-nitrosyl complexes and their relation to O₂ activation by nonheme iron enzyme active sites. *J. Am. Chem. Soc.* 117, 715–732.
 41. Varotsis, C., Ohta, T., Kitagawa, T., Soulimane, T., and Pinakoulaki, E. (2007) The structure of the hyponitrite species in a heme Fe-Cu binuclear center. *Angew. Chem., Int. Ed.* 46, 2210–2214.
 42. Miller, L. M., Pedraza, A. J., and Chance, M. R. (1997) Identification of conformational substates involved in nitric oxide binding to ferric and ferrous myoglobin through difference Fourier transform infrared spectroscopy (FTIR). *Biochemistry* 36, 12199–12207.
 43. Wildschut, J. D., Lang, R. M., Voordouw, J. K., and Voordouw, G. (2006) Rubredoxin: oxygen oxidoreductase enhances survival of *Desulfovibrio vulgaris* Hildenborough under microaerophilic conditions. *J. Bacteriol.* 188, 6253–6260.
 44. Rodrigues, R., Vicente, J. B., Félix, R., Oliveira, S., Teixeira, M., and Rodrigues-Pousada, C. (2006) *Desulfovibrio gigas* flavodiiron protein affords protection against nitrosative stress in vivo. *J. Bacteriol.* 188, 2745–2751.
 45. Silaghi-Dumitrescu, R., Ng, K. Y., Viswanathan, R., and Kurtz, D. M., Jr. (2005) A flavo-diiron protein from *Desulfovibrio vulgaris* with oxidase and nitric oxide reductase activities. Evidence for an in vivo nitric oxide scavenging function. *Biochemistry* 44, 3572–3579.

46. Victor, B. L., Baptista, A. M., and Soares, C. M. (2009) Dioxxygen and nitric oxide pathways and affinity to the catalytic site of rubredoxin: oxygen oxidoreductase from *Desulfovibrio gigas*. *J. Biol. Inorg. Chem.* **14**, 853–862.
47. Feig, A. L., Bautista, M. T., and Lippard, S. J. (1996) A carboxylate-bridged non-heme diiron dinitrosyl complex. *Inorg. Chem.* **35**, 6892–6898.
48. Adams, H., Bailey, N. A., Debaecker, N., Fenton, D. E., Kanda, W., Latour, J.-M., Okawa, H., and Sakiyama, H. (1997) A dinuclear (μ -carboxylato)manganese(II) complex derived from a macrocyclic ligand: A structural model for active sites in natural systems. *Angew. Chem., Int. Ed.* **33**, 2535–2537.
49. Samples, C. R., Howard, T., Raushel, F. M., and DeRose, V. J. (2005) Protonation of the binuclear metal center within the active site of phosphotriesterase. *Biochemistry* **44**, 11005–11013.
50. Lis, T., and Matuszewski, J. (1979) Manganese(II) malonate dihydrate: A reinvestigation. *Acta Crystallogr. B* **35**, 2212–2214.
51. Rodriguez-Martin, Y., Hernandez-Molina, M., Sanchiz, J., Ruiz-Perez, C., Lloret, F., and Julve, M. (2003) Crystal structure and magnetic properties of two- and three-dimensional malonato-bridged manganese(II) complexes. *Dalton Trans.*, 2359–2365.
52. Clay, M. D., Cosper, C. A., Jenney, F. E., Jr., Adams, M. W., and Johnson, M. K. (2003) Nitric oxide binding at the mononuclear active site of reduced *Pyrococcus furiosus* superoxide reductase. *Proc. Natl. Acad. Sci. U.S.A.* **100**, 3796–3801.
53. Orville, A. M., and Lipscomb, J. D. (1993) Simultaneous binding of nitric oxide and isotopically labeled substrates or inhibitors by reduced protocatechuate 3,4-dioxygenase. *J. Biol. Chem.* **268**, 8596–8607.
54. (a) Olson, L. W., Schaeper, D., Lançon, D., and Kadish, K. M. (1982) Characterization of several novel iron nitrosyl porphyrins. *J. Am. Chem. Soc.* **104**, 2042–2044. (b) Lançon, D., and Kadish, K. M. (1983) Electrochemical and spectral characterization of iron mono- and dinitrosyl porphyrins. *J. Am. Chem. Soc.* **105**, 5610–5617. (c) Pellegrino, J., Bari, S. E., Bikiel, D. E., and Doctorovich, F. (2010) Successful stabilization of the elusive species $\{\text{FeNO}\}^8$ in a heme model. *J. Am. Chem. Soc.* **132**, 989–995.
55. (a) Lin, R., and Farmer, P. J. (2000) The HNO adduct of myoglobin: Synthesis and characterization. *J. Am. Chem. Soc.* **122**, 2393–2394. (b) Kumar, M. R., Pervitsky, D., Chen, L., Poulos, T., Kundu, S., Hargrove, M. S., Rivera, E. J., Diaz, A., Colon, J. L., and Farmer, P. J. (2009) Nitrosyl hydroxide (HNO) as an O_2 analogue: Long-lived HNO adducts of ferrous globins. *Biochemistry* **48**, 5018–5025.
56. (a) Hauser, C., Glaser, T., Bill, E., Weyhermüller, T., and Wieghardt, K. (2000) The electronic structures of an isostructural series of octahedral nitrosyliron complexes $\{\text{Fe-NO}\}^{6,7,8}$ elucidated by Mössbauer spectroscopy. *J. Am. Chem. Soc.* **122**, 4352–4365. (b) Serres, R. G., Grapperhaus, C. A., Bothe, E., Bill, E., Weyhermüller, T., Neese, F., and Wieghardt, K. (2004) Structural, spectroscopic, and computational study of an octahedral, non-heme $\{\text{Fe-NO}\}^{6-8}$ series: $[\text{Fe}(\text{NO})(\text{cyclam-ac})]^{2+/+/0}$. *J. Am. Chem. Soc.* **126**, 5138–5153.
57. Montenegro, A. C., Amorebieta, V. T., Slep, L. D., Martin, D. F., Roncaroli, F., Murgida, D. H., Bari, S. E., and Olabe, J. A. (2009) Three redox states of nitrosyl: NO^+ , NO^\bullet , and NO^- /HNO interconvert reversibly on the same pentacyanoferrate(II) platform. *Angew. Chem., Int. Ed.* **48**, 4213–4216.